Check for updates

3D macroporous TiO$_2$ inverse opal binary and ternary composite materials and their photocatalytic activity†

Daniel A. Corella and Bharat Baruah [ID] *

This work reports the design of binary and ternary thin film based photocatalysts consisting of 3D macroporous inverse opal (IO) titanium dioxide, IO-TiO$_2$, embedded with gold nanoparticles (AuNPs) and cadmium sulfide (CdS) thin film. The composite materials thus created are IO-TiO$_2$–AuNPs, IO-TiO$_2$–CdS, and IO-TiO$_2$–AuNPs–CdS. The IO-TiO$_2$ 3D macroporous films are obtained by a liquid phase co-assembly method consisting of the simultaneous self-assembly of polystyrene (PS) nanospheres with a water soluble titania precursor. AuNPs and CdS thin films are integrated to the above IO-TiO$_2$ by *in situ* synthesis and successive ionic layer adsorption and reaction (SILAR) methods, respectively. The composite materials demonstrated very good photocatalytic proficiency against an organic pollutant analog under UV and visible lighting conditions. The morphologies of the photocatalysts were imaged with scanning electron microscopy (SEM). The elemental components were determined using energy dispersive X-ray (EDX) line analysis, and Raman spectroscopy. UV-visible spectroscopy was used to assess the photocatalytic efficiency of the composites in decomposing organic pollutant analog.

1. Introduction

Extensive use of organic dyes in industries such as food and drug manufacturing, textiles, paper, pigments, leather, and cosmetics led to water pollution.[1] Most of such dyes and their metabolites are toxic and carcinogenic and tend to create water contamination and thereby endanger public health as well as imposing harmful consequences upon the ecosystem.[2–6] In recent years, the development of energy efficient photocatalysts has been a very intense area of research to treat industrial wastewater containing harmful aromatic compounds and organic dyes. Titanium(IV) oxide is one such photocatalyst that is renowned for being cheap, chemically stable, and non-toxic.[7] Titania has been used in dye-sensitized solar cells,[8,9] anti-fogging coatings[10] for glass and degradation of herbicides and dyes.[11,12] Due to its large band gap (≈ 3.2 eV) TiO$_2$ is mostly active in ultra violet light.[13] TiO$_2$ has been coupled to a narrow band gap semiconductor with a conductive mediator such as gold nanoparticles that exhibit surface plasmon resonance (SPR),[14,15] and this allows easy electron transfer from the conduction band of TiO$_2$ to the target for reduction and minimizes the risk of electron–hole recombination.[16] Besides the use of compositional variation, one of the possible structural

alteration to enhance photocatalytic activity is the use of three dimensionally (3D) ordered macroporous photonic crystals also known as inverse opal (IO).[17–20] IO photonic crystals have photonic band gaps and have a distinct way of steering light propagation through them. That is why they demonstrate distinctive optical characteristics and structural features namely, slow photon,[17,21,22] large surface area,[23] and multiple scattering. These properties have been utilized in solar cells,[24] polarizers,[25] sensors,[26] and photocatalysis.[27] Photocatalyst fabricated using IO type photonic crystals have high surface : volume ratio due to the presence of interconnected pores, which enables light harvesting and mass transfer. Inverse opal photonic crystals have another characteristic feature known as photonic band gap (PBG), due to which certain frequencies of light circulation is forbidden analogous to electronic band gap where electron flow is regulated in a semiconductor.[21] Therefore in inverse opal photonic crystals, the photons are slowed down near the edges of the PBG and thereby localized in the area of activity of the material enhancing the efficiency of photocarrier generation.

Very recently Zhao *et al.* synthesized silver nanoparticles (AgNPs) on IO-TiO$_2$ and demonstrated enhanced visible light driven photocatalytic activity.[15] The photocatalytic enhancement for methylene blue degradation was attributed to the synergistic effect of optimized AgNPs deposition and an ordered macroporous IO-TiO$_2$ morphology. Lu and co-workers integrated AuNPs into photonic crystals of TiO$_2$ and demonstrated synergistic enhancement of light harvesting due to the localized surface plasmon resonance (LSPR) of AuNPs.[14] The photonic

Department of Chemistry and Biochemistry, Kennesaw State University, Kennesaw, GA 30144-5591, USA. E-mail: bbaruah@kennesaw.edu; Fax: +1 470 578 9137; Tel: +1 470 578 2654

effect of IO-TiO$_2$ intensify the LSPR by matching the photonic band gap (PBG) with the wavelength of plasmonic absorption.[14] The efficient pollutant degradation is caused by reactive oxygen species (ROS), which are formed due to the electroreduction of dissolved oxygen with the photogenerated electrons.[28,29]

Thirdly, the inadequate use of solar light by TiO$_2$ alone to function as an efficient photocatalyst can be improved by combining it with a narrow band gap semiconductors.[30] Commonly used narrow band gap semiconductors include CuInS$_2$,[31] Cu$_2$O,[32] ZnFe$_2$O$_4$,[33] CdS,[34,35] etc. Among these CdS is the most favorable paring material since it has a narrow band gap of 2.40 eV allowing for a longer excitation wavelength (<516 nm) and more efficient absorption of visible light.[36] In the binary system, TiO$_2$–CdS reported by Pant and co-workers[34] the TiO$_2$ nanoparticles were embedded in carbon nanofibers using the electrospinning process with subsequent calcination in the presence of argon. They claim that this strategy enables better adsorption and fast decay of the dye under visible light.[34] In another recent report, Zhang et al.[37] demonstrated controlled self-assembly of CdS nanospheres (NSPs) on TiO$_2$ nanobelts (TNBs) purely based on electrostatic attractive forces. The prepared binary 1D TNBs/3D CdS NSPs composite material depicted tremendous photocatalytic activity compared to the TNBs and CdS NSPs under visible light.[37] The formation of binary hetero conjugate between TNBs and CdS NSPs improved the electron–hole life time and thereby enhanced the photocatalytic degradation of the dye. This indicated that such fabrication has future implications in boosting photocatalytic activity of binary heterocomposite materials.[37] Zhao et al. recently fabricated a ternary system consisting of TiO$_2$–Au–CdS powder where TiO$_2$ was 3D macroporous inverse opal.[13] They demonstrated that incorporation of AuNPs and CdS into a ternary system was able to enhance the separation of the photogenerated electrons and holes.[13] The ternary system also compensated for the UV-light restrictions that is a weakness of TiO$_2$.[13] Under ultraviolet-visible light, the photogenerated electrons in TiO$_2$ would be transferred to recombine with the holes of CdS, and under visible light electrons would move to the conduction band (CB) of TiO$_2$ from CdS via AuNPs.[13] In summary, in this ternary system the AuNPs acted as a mediator between TiO$_2$ and CdS and helped transfer the photogenerated electrons and produced more active sites for reducing H$^+$ to H$_2$.[13] Kim and co-workers demonstrated that the ternary system containing core–shell Au@CdS on TiO$_2$ nanofibers (TNF) has tremendous potential for low-cost and clean hydrogen production.[38] The comparison of photocatalytic results showed that the Au@CdS/TNF has better efficiency in H$_2$ production than the Au@CdS/P25 where P25 is commercially available TiO$_2$ in the presence of visible light.[38] Also, the core–shell Au@CdS prevented formation CdSO$_4$ from CdS thus preserving the photocatalytic activity.[38]

In this report, we fabricated a ternary thin film system containing inverse opal TiO$_2$ (IO-TiO$_2$), AuNPs and CdS thin film on a glass substrate, IO-TiO$_2$–AuNPs–CdS. We investigated the photocatalytic degradation of the diazo dye trypan blue (TB) under visible light and UV light irradiation. Also, we have fabricated the binary systems such as IO-TiO$_2$–AuNPs and IO-TiO$_2$–CdS to compare the photocatalytic activity with the ternary system. We employed various imaging and surface analysis techniques to understand the differed photocatalytic activities of the binary and ternary systems. We however, use thin films of the IO-TiO$_2$ on a glass slide in our binary and ternary systems as opposed to powdered form of the IO-TiO$_2$, commonly seen in the literature[13,29,38–40] to facilitate ease of extraction of the catalyst systems from aqueous media after the reaction. Inspired by the available literature results in photocatalytic activity of IO-TiO$_2$ systems and corresponding binary and ternary systems, this work is an effort to shed light on the development of photocatalysts by combining wide band-gap semiconductor with narrow band-gap semiconductor as well as plasmonic nanoparticles.

2. Results and discussion

2.1 Design and fabrication

This report demonstrates the fabrication of binary and ternary thin film photocatalyst by four step and five step methods, respectively. The design and fabrication of the different IO-TiO$_2$ based composite materials on a glass slide are schematically depicted in Fig. 1. First IO-TiO$_2$ were created by evaporating a coassembly[41,42] mixture of polystyrene (PS) and titanium(iv) bis(ammonium lactate)dihydroxide (TiBALDH) in water onto a vertically standing glass slide in a 45 °C incubator for 1–2 days. Subsequently, the slides were calcined at 500 °C for 3 hours in a muffle furnace and were left to cool naturally to room temperature (Fig. 1). The obtained IO-TiO$_2$ composite materials were soaked in a NaAuCl$_4$ solution, and the adsorbed anions containing Au^{3+} were further reduced to AuNPs with ascorbic acid thereby generating IO-TiO$_2$–AuNPs. Finally, SILAR method[43,44] was used with slight modification of the literature method to incorporate CdS thin film into IO-TiO$_2$ and IO-TiO$_2$–AuNPs and plain glass slide creating IO-TiO$_2$–CdS, IO-TiO$_2$–AuNPs–CdS, and CdS film on glass slide.

2.2 Morphology, SEM images and EDX analysis of the composites

The surface morphologies of the glass slide based composite materials are imaged by Topcon DS150 Field Emission Scanning Electron Microscope (FESEM) as depicted in Fig. 2. Fig. 2a and b present PS film and bare IO-TiO$_2$, respectively. The sizes of the PS spheres were measured to be 272 nm, and a light green iridescence is observed on the digital image of the film shown in the inset of Fig. 2a. The bare IO-TiO$_2$ slide appears white. The CdS thin film on the glass slide are shown in Fig. 2c, and the digital image shown in the inset is yellow. The Fig. 2d and e present the binary systems of IO-TiO$_2$–AuNPs and IO-TiO$_2$–CdS, respectively. IO-TiO$_2$–AuNPs is created by the in situ synthesis of AuNPs on IO-TiO$_2$ in water. Due to the presence of AuNPs, the color turned reddish-purple from white. IO-TiO$_2$–CdS is formed by depositing CdS on IO-TiO$_2$ by SILAR method[43,44] and the color of the slide turned yellow. Finally, the ternary system IO-TiO$_2$–AuNPs–CdS was shown in Fig. 2f. The digital image appeared greenish-black. The SEM image was analyzed with image J
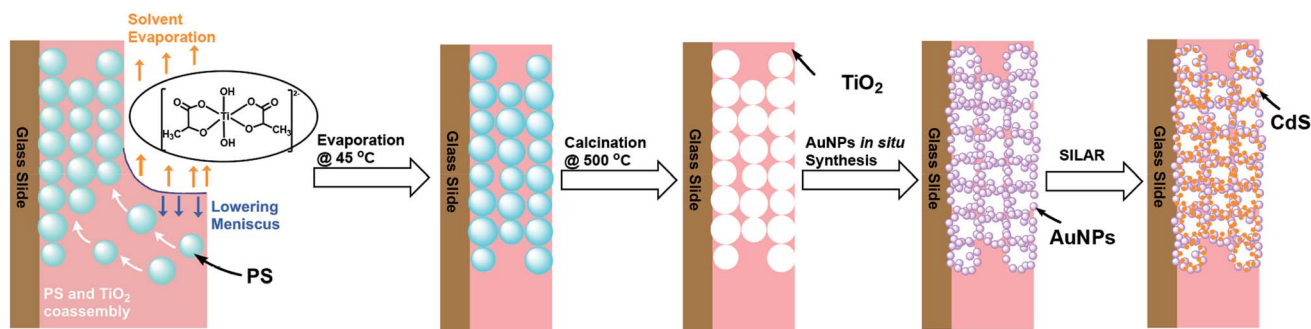
Fig. 1 Schematic representation of fabrication of inverse opal TiO_2, IO-TiO_2, binary IO-TiO_2–AuNPs and ternary IO-TiO_2–AuNPs–CdS composite materials on glass slides. Approximately 272 nm PS sphere and TiBALDH co-assembly was used to generate the template for the inverse opal. AuNPs were synthesized following *in situ* method and CdS thin film were incorporated using SILAR technique.

software, and average size distribution of the AuNPs are presented in Fig. S2 (ESI).† The inverse opal structures are deformed due to the contraction and expansion during the cooling and heating process. Large area SEM images are shown in the ESI (Fig. S3).†

The signals for elemental Ti, Au, Cd, S and O are presented in the EDX spectra in Fig. 3. In the spectrum of IO-TiO_2 (Fig. 3, black line) the signal at 4.49 keV is clear indication of the presence of Ti. This signal is prominent in the spectra of IO-TiO_2–AuNPs (blue line), IO-TiO_2–CdS (pink line), and IO-TiO_2–AuNPs–CdS (green line) as shown in Fig. 3 indicating the presence of Ti. Similarly, the signal at 0.53 keV is due to the presence of O in all the above samples. Cd signals appear at 3.14 and 3.32 and S signal appears at 2.30 keV. These are only visible in samples CdS (red line), IO-TiO_2–CdS (pink line), and IO-TiO_2–

AuNPs–CdS (green line) in Fig. 3. Finally, Au signal at 2.13 keV is observed only in IO-TiO_2–AuNPs (blue line), and IO-TiO_2–AuNPs–CdS (green line) composites. Also, two more prominent signals at 1.04 and 1.74 keV indicate the presence of Na and Si, respectively, and are seen most probably due to the glass substrate.

2.3 Optical absorbance

Fig. 4 demonstrates the solid-state UV-visible absorption spectra of IO-TiO_2 (black line), CdS (red line), IO-TiO_2–AuNPs (blue line), IO-TiO_2–CdS (pink line), and IO-TiO_2–AuNPs–CdS. The bare IO-TiO_2 shows strong absorbance below 400 nm.[13] The pure CdS thin film show absorbance at around 500 nm. In the case of binary IO-TiO_2–AuNPs composite a broad signal is observed

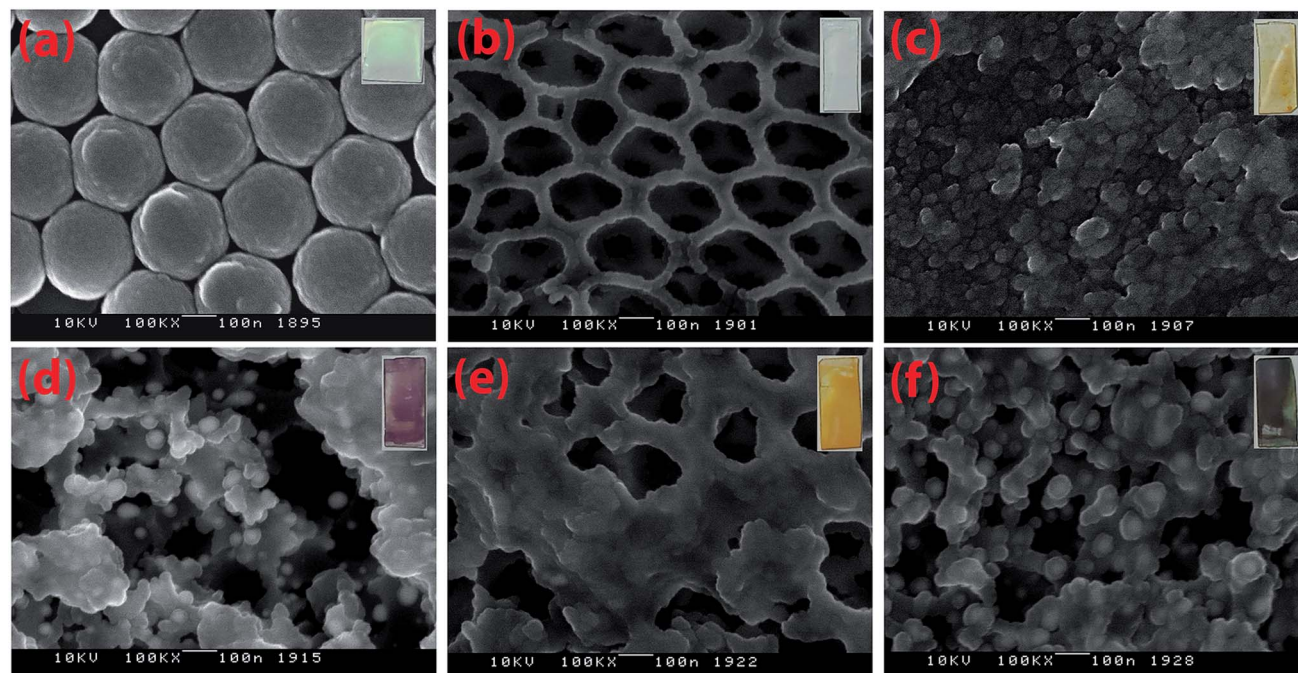**Fig. 2** SEM images of PS film (a), IO-TiO_2 (b), CdS (c), IO-TiO_2–AuNPs (d), IO-TiO_2–CdS (e), and IO-TiO_2–AuNPs–CdS (f) are shown (scale bar is 100 nm). Images were taken with Topcon DS150 Field Emission Scanning Electron Microscope. Digital photographs of each of these composites are shown in the inset.
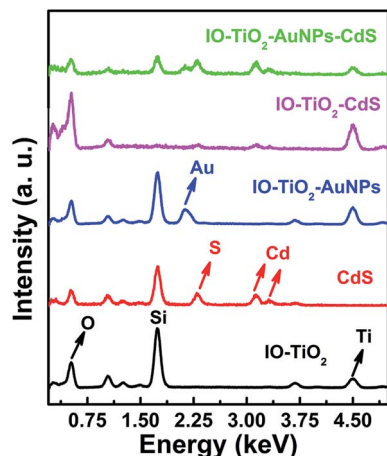
Fig. 3 The EDX spectra of IO-TiO$_2$ (black line), CdS (red line), IO-TiO$_2$–AuNPs (blue line), IO-TiO$_2$–CdS (pink line), and IO-TiO$_2$–AuNPs–CdS (green line) are shown in here. Data was acquired using JEOL JSM5800LV SEM EDX at an accelerating voltage of 10 keV.
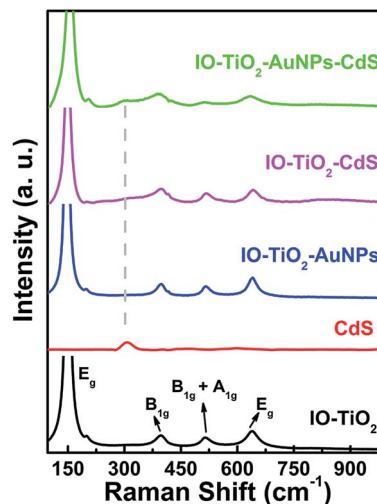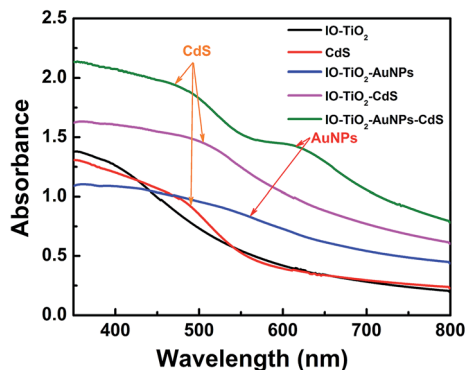

Fig. 4 The UV-visible spectra of IO-TiO$_2$ (black line), CdS (red line), IO-TiO$_2$–AuNPs (blue line), IO-TiO$_2$–CdS (pink line), and IO-TiO$_2$–AuNPs–CdS (green line) are shown in here.

around 550 nm, due to the expansion of the absorption of the composite by the surface plasmon resonance (SPR) of the plasmonic AuNPs.[13] Such plasmonic expansion can be revamped by altering the size, and shape of plasmonic nanoparticles.[45,46] The absorption maximum at ~520 nm in IO-TiO$_2$–CdS indicates the sensitization of TiO$_2$ absorption by CdS, and this corresponds to literature report.[13,47] In IO-TiO$_2$–AuNPs–CdS the presence of both plasmonic AuNPs and narrow band-gap semiconductor CdS the SPR band red shifted to ~650 nm due to the robust electromagnetic pairing of AuNPs and CdS.[13,48] The direct contact of AuNPs with CdS having higher dielectric constant compared to air would cause red shift of the SPR band.[13,49]

2.4 Raman spectroscopic characterization of the composites

In order to determine the phase composition, Raman spectra of different composite materials are collected.[38,50] Fig. 5 shows four characteristic signals at 146, 394, 514, and 639 cm^{-1} assigned to E$_g$, B$_{1g}$, B$_{1g}$ + A$_{1g}$ and E$_g$, respectively, confirming anatase-phase of TiO$_2$ (ref. 38 and 51) in four composites

Fig. 5 The Raman spectra of the as prepared different composite materials: IO-TiO$_2$ (black line), CdS (red line), IO-TiO$_2$–AuNPs (blue line), IO-TiO$_2$–CdS (pink line), and IO-TiO$_2$–AuNPs–CdS (green line).

namely IO-TiO$_2$ (black line), binary IO-TiO$_2$–AuNPs (blue line), binary IO-TiO$_2$–CdS (pink line) and ternary IO-TiO$_2$–AuNPs–CdS (green line). There are no additional signals at 234, 447, and 612 cm^{-1} corresponding to B$_{1g}$, E$_g$, and A$_{1g}$ modes, respectively, of the rutile phase of TiO$_2$. In bare CdS film, the characteristic signal at 306 cm^{-1} is observed.[38] In the case of IO-TiO$_2$–CdS and IO-TiO$_2$–AuNPs–CdS the characteristic signal for CdS at 306 cm^{-1} appear as a shoulder to the B$_{1g}$ mode of the anatase-phase TiO$_2$.[38] The other signal of CdS at ~603 cm^{-1} is very broad and buried in the baseline.

2.5 Photocatalytic reactions by the composites in visible light

As depicted in Fig. 4, due to the incorporation of AuNPs and CdS the light absorption range of the ternary system, IO-TiO$_2$–AuNPs–CdS has widened from UV region to visible region.[29] This would invigorate the photocatalytic activity of ternary system under visible light.[29] Photocatalytic degradation of trypan blue (TB) by the composite materials were first assessed under visible light. The TB sample was kept in the dark for 30 minutes before irradiating with visible light. The UV-visible absorbance of TB against wavelength and the corresponding degradation against time were presented in Fig. 6. Fig. 6A shows the absorbance of 20 μM TB against wavelength in the presence of IO-TiO$_2$–AuNPs–CdS under visible light irradiation. During the 120 min, total irradiation the IO-TiO$_2$ composite depicted lowest photocatalytic enhancement because of zero visible light response (Fig. 6B). IO-TiO$_2$–AuNPs composite depicted no photocatalytic enhancement like the IO-TiO$_2$(Fig. 6B and C). This lack of enhancement is attributed to the larger size of the AuNPs[14] (50 nm, see Fig. S2†). Next the bare CdS thin film shows better activity than IO-TiO$_2$ and IO-TiO$_2$–AuNPs due to its intrinsic enhanced visible light response. Finally, the photocatalytic activity of binary IO-TIO$_2$–CdS and ternary IO-TiO$_2$–AuNPs–CdS are not significantly different but far superior to the
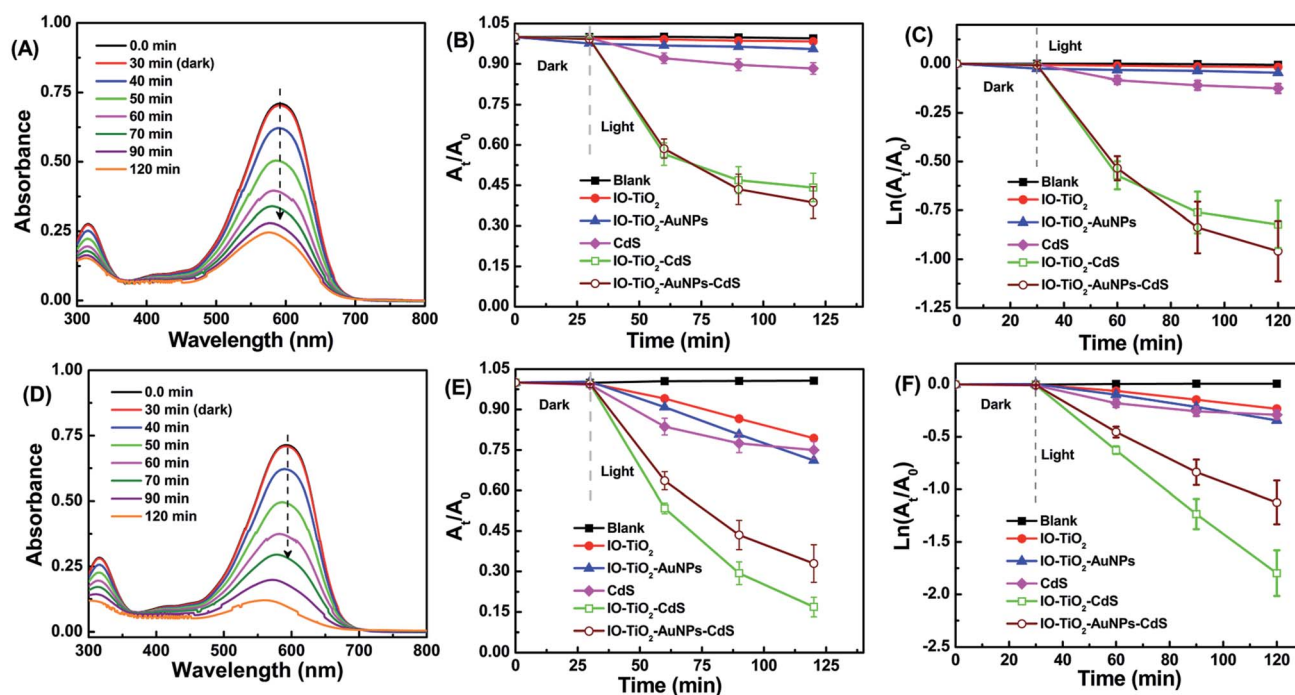
Fig. 6 Plot of UV-visible absorbance of 20 μM TB against wavelength are shown in (A) and (D). The absorbance at 592 nm continuously decrease due to catalytic activity of IO-TiO$_2$–AuNPs–CdS composite under visible light irradiation (A) and IO-TiO$_2$–CdS composite under UV light irradiation (D). Also, presented photocatalytic degradation TB using various photocatalyst under visible light (B and C) and under UV light (E and F).

other composites. Unfortunately, the photocatalytic activity of AuNPs loaded ternary composite IO-TiO$_2$–AuNPs–CdS was not significantly improved to fulfill the real-world urge. As the *in situ* synthesized nanoparticles are ∼50 nm (Fig. S2†),[14] they are unable to enhance the photocatalytic activity of the ternary system, TiO$_2$–AuNPs–CdS. However, the presence of CdS loading astoundingly improved the visible light driven photocatalysis in binary IO-TiO$_2$–CdS and ternary IO-TiO$_2$–AuNPs–CdS.[29] CdS was used in combination of TiO$_2$ due to its narrow band gap (2.4 eV) as this could enlarge the light response range of TiO$_2$ to visible region. In the presence of the visible light, the photogenerated electrons of CdS move from the CB of CdS to the CB of TiO$_2$ in a binary system, IO-TiO$_2$–CdS (Fig. 7C). On the other hand, in the ternary system, IO-TiO$_2$–AuNPs–CdS the mediator AuNPs would help in the process (Fig. 7A). However, the CdS thin film underwent photocorrosion under the visible light irradiation as S^{2-} ions get oxidized to elementary sulfur or oxidized species of sulfur by the photogenerated holes[29] as can be visualized by the loss of activity over time in the CdS containing systems and the digital pictures of the slides in Fig. S4.† Thus, these composites IO-TiO$_2$–CdS and IO-TiO$_2$–AuNPs–CdS were unable to demonstrate recyclability of photocatalytic reaction.[29] As shown in the Fig. 6C the plot of ln(A_t/A_0) against time are not linear and the degradation reaction do not follow pseudo-first order kinetics.

2.6 Photocatalytic reactions of the composites in UV light

The ternary system IO-TiO$_2$–AuNPs–CdS is also known as Z-scheme where CdS, IO-TiO$_2$ and AuNPs are photosensitizer I

(PSI), photosensitizer II (PSII), and electron mediator, respectively.[38,52] Therefore, we compared the photocatalytic degradation of TB under UV (λ = 365 nm) irradiation as presented in Fig. 6(D–F). Fig. 6D depicts the absorbance of 20 μM TB against wavelength in the presence of IO-TiO$_2$–CdS under UV light irradiation. During the 120 min, total irradiation the IO-TiO$_2$ composite showed the lowest photocatalytic activity. However, this result is much better than IO-TiO$_2$ under visible light (Fig. 6A) as TiO$_2$ itself is much more active under UV light.[38] The IO-TiO$_2$–AuNPs composite shows almost similar dye degradation within the experimental error. Bare CdS performed very similar to that of IO-TiO$_2$ and IO-TiO$_2$–AuNPs. Among the binary IO-TiO$_2$–CdS and ternary IO-TiO$_2$–AuNPs–CdS, the former performed much better than the ternary system (Fig. 6E and F). Both IO-TiO$_2$–CdS and IO-TiO$_2$–AuNPs–CdS performed considerably better than that under visible light (Fig. 6B). In the presence of the UV light, the photogenerated electrons of TiO$_2$ move from the CB of TiO$_2$ to the CB of CdS in a binary system, IO-TiO$_2$–CdS (Fig. 7D). On the other hand, in the ternary system, IO-TiO$_2$–AuNPs–CdS the mediator AuNPs would help in the process (Fig. 7B). In summary, the binary IO-TiO$_2$–CdS is much more active photocatalyst under UV light than in visible light.

The kinetics of the photocatalytic degradation of TB under UV light can be evaluated following the Langmuir–Hinshelwood first-order model shown in eqn (1).[53] Here "k" is first order rate constant and "t" is the time in min.
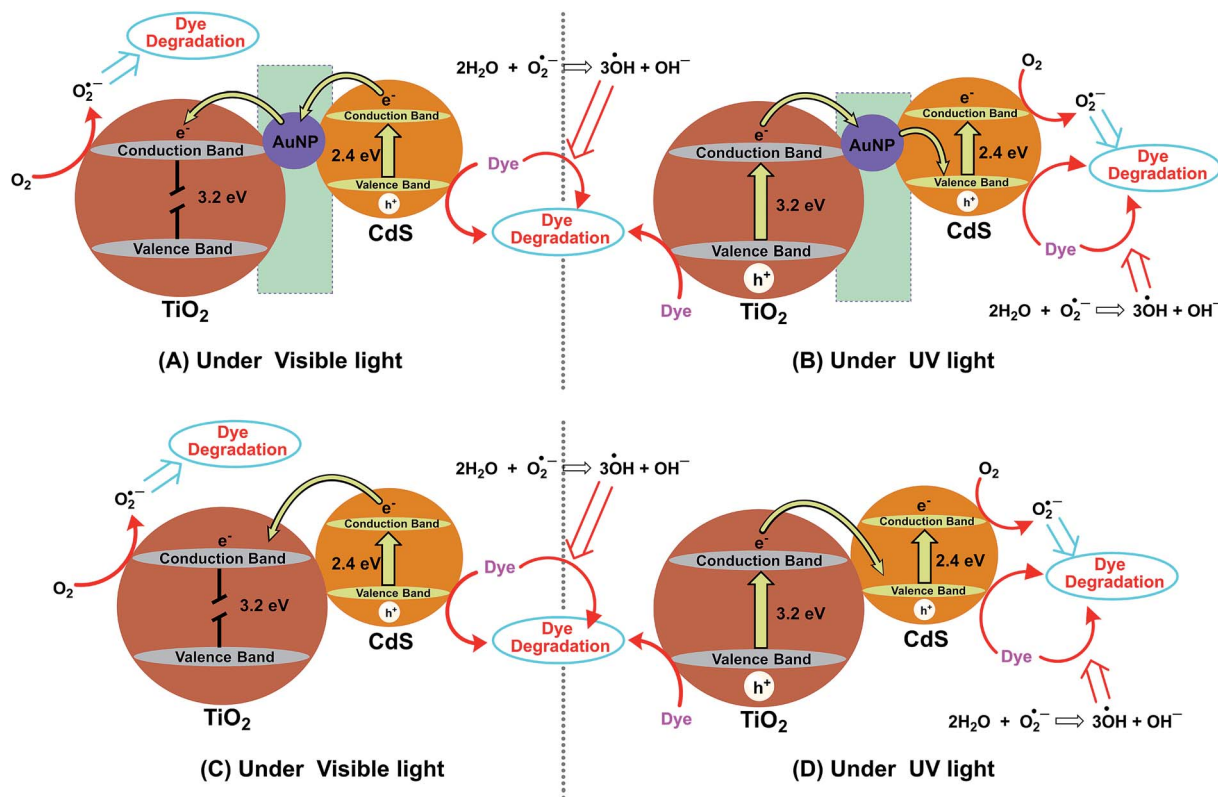
$$\ln(A_t/A_0) = -kt \tag{1}$$

Fig. 7 Proposed photocatalytic mechanism of TB degradation over IO-TiO$_2$–AuNPs–CdS (A and B) and IO-TiO$_2$–CdS (C and D) under visible irradiation (A and C) and under UV light irradiation (B and D).

The relationship of $\ln(A_t/A_0)$ against time over various photocatalysts are shown in Fig. 6F. The degradation kinetic parameter is shown in Table 1. The R^2 values are indicative of the fact that the degradation process follows Langmuir–Hinshelwood first-order model.[53] Based on the data tabulated in Table 1 the rate of TB degradation over IO-TiO$_2$–CdS is 0.0206 min^{-1} and is approximately 7.9, 5.4, 5.7 and 1.5 times the rates of IO-TiO$_2$ (0.0026 min^{-1}), IO-TiO$_2$–AuNPs (0.0038 min^{-1}), CdS (0.0036 min^{-1}) and IO-TiO$_2$–AuNPs–CdS (0.0140 min^{-1}), respectively under UV light.

2.7 Mechanism of photocatalytic degradation

The possible photocatalytic degradation mechanism of TB under visible light is illustrated in Fig. 7A. When IO-TiO$_2$–AuNPs–CdS composite is illuminated with visible light, an

electron (e$^-$) in the valence band (VB) of CdS would be promoted to the conduction band (CB) generating electron/hole pair.[28,29] Subsequently the electrons will be trapped in the AuNPs and will be further transferred to IO-TiO$_2$ CB. The electron in IO-TiO$_2$ CB can react with dissolved oxygen to form active oxygen species (O$_2^-$·) which can further react with water to generate OH· radicals.[28] The hole (h$^+$) in CdS VB could also react with OH$^-$ to generate OH· radicals (Fig. 7A). The hole, and generated O$_2^-$·, and OH· radicals are responsible for degradation of TB.[28,54,55] The possible photocatalytic degradation reactions are presented below:

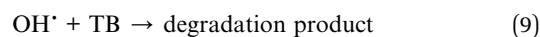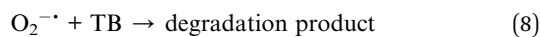$$CdS + h\nu \rightarrow CdS\ (e^- + h^+)\ (\text{visible light}) \tag{2}$$

$$TiO_2 + h\nu \rightarrow TiO_2\ (e^- + h^+)\ (\text{UV light}) \tag{3}$$

$$e^- + O_2 \rightarrow O_2^-· \tag{4}$$

$$O_2^-· + 2H_2O \rightarrow 3OH· + OH^- \tag{5}$$

$$h^+ + OH^- \rightarrow OH· \tag{6}$$

$$h^+ + TB \rightarrow \text{degradation product} \tag{7}$$

$$O_2^-· + TB \rightarrow \text{degradation product} \tag{8}$$
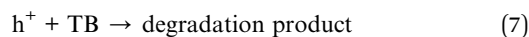
$$OH· + TB \rightarrow \text{degradation product} \tag{9}$$

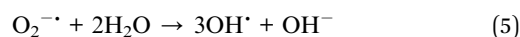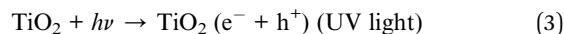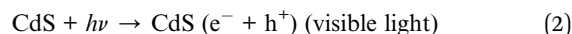**Table 1** Pseudo-first order degradation kinetic parameter of TB over IO-TiO$_2$, IO-TiO$_2$–AuNPs, CdS, IO-TiO$_2$–CdS, and IO-TiO$_2$–AuNPs–CdS under UV light

Sample	k (min^{-1})	R^2
IO-TiO$_2$	−0.0026	0.9888
IO-TiO$_2$–AuNPs	−0.0038	0.9954
CdS	−0.0036	0.9302
IO-TiO$_2$–CdS	−0.0206	0.9997
IO-TiO$_2$–AuNPs–CdS	−0.0140	0.9923

To further investigate the effect of incident light we have performed additional photocatalytic experiments in the presence of UV light, and the electron transfer process is illustrated in Fig. 7B. Under UV irradiation the IO-TiO$_2$–AuNPs–CdS composite apparently shows better photocatalytic degradation (Fig. 6E and F) of the TB. In this system, under UV light both IO-TiO$_2$ and CdS provide electron/hole pair.[13] Under UV light the photogenerated electrons of IO-TiO$_2$ would first transfer to AuNPs and then to the valence band of CdS, and then further get excited to the CB of CdS. This creates a typical electron-transfer route of Z-scheme photocatalyst.[13,50,56] As shown in Fig. 7B the reduction would occur at the CB of CdS and oxidation would occur at the VB of IO-TiO$_2$ generating superoxide (O$_2^{-\cdot}$) and hydroxyl radicals (OH$^\cdot$), respectively. The dye reduction may proceed in the VB of IO-TiO$_2$; however, the CB of CdS is highly negative compared to that of IO-TiO$_2$, CdS has better reducing power and dye reduction may be enhanced due to the presence of this Z-scheme pathway under the irradiation of the UV light.[13,50,56] In this case effective dye degradation may happen in VB of IO-TiO$_2$, CB of CdS and VB of CdS. Hence, the photocatalytic activity of ternary IO-TiO$_2$–AuNPs–CdS is superior to that of visible light irradiation (Fig. 7C). It is known in the literature that the photocatalytic performance could be improved by SPR of AuNPs.[57] However, for our ternary composite, IO-TiO$_2$–AuNPs–CdS the photocatalysis under visible light is comparable to that of binary, IO-TiO$_2$–CdS (Fig. 6B and C). This indicated that SPR could not enhance the photocatalytic activity of our ternary composite, IO-TiO$_2$–AuNPs–CdS[13] as the *in situ* synthesized nanoparticles are ~50 nm (Fig. S2†).[14] On the contrary, under UV light the binary IO-TiO$_2$–CdS is much active than the ternary IO-TiO$_2$–AuNPs–CdS (Fig. 6E and F). Further investigation is needed to evaluate the contribution of the AuNPs' SPR in the photocatalytic behavior of the ternary composite, IO-TiO$_2$–AuNPs–CdS. Photocatalytic reactions and formation of reactive oxygen species are shown in eqn (2)–(9). Fig. 7C and D represent the dye degradation mechanism of binary system, IO-TiO$_2$–CdS under visible light and UV light, respectively.

2.8 Radical trapping experiment

We performed trapping experiments to understand which radical is main oxidative species in degrading the TB. As discussed in the previous section h$^+$, O$_2^{\cdot-}$, and $^\cdot$OH could be active species in the degrading the dye. We utilized EDTA, BQ, and *t*-BuOH as our scavengers for h$^+$, O$_2^{\cdot-}$, and $^\cdot$OH, respectively.[55,58–60] A certain amount of these scavenger molecules were added to a representative photocatalytic reaction mixture in the presence of IO-TiO$_2$–CdS. Fig. 8 demonstrates the photocatalytic degradation of TB in the presence of EDTA, BQ, and *t*-BuOH scavengers. As evident from Fig. 8, the addition of EDTA and BQ lead to a significant slowdown of the photocatalytic degradation of TB under UV light. However, in the presence of *t*-BuOH, there is no significant loss of activity. This result urges the fact that the hydroxyl radical is not the primary cause of TB degradation under UV light. The h$^+$ and the O$_2^{\cdot-}$

species play a dominant role in the photocatalytic degradation of TB under UV light.

2.9 Binary and ternary synergistic effect

To demonstrate the synergistic effect of incorporating the photosensitizers into binary and ternary systems, percent degradation of the dyes was compared. Percent degradation was defined per eqn (10):

$$\% \text{ degradation} = \left(1 - \frac{A_t}{A_0}\right) \times 100\% \qquad (10)$$

Percent degradation for the two unary systems, IO-TiO$_2$ and CdS, and binary IO-TiO$_2$–AuNPs plus IO-TiO$_2$–CdS were summed together and plotted in Fig. 9 along with percent degradation for the binary IO-TiO$_2$–CdS and ternary IO-TiO$_2$–Au–CdS composites. What is notable is the rate of dye degradation for both the binary IO-TiO$_2$–CdS and ternary IO-TiO$_2$–AuNPs–CdS systems exceed the rate of degradation for their constituent parts summed together. This demonstrates that improved photocatalytic performance due to incorporation of photosensitizers into binary and ternary systems is more than simply a result of both sensitizers working simultaneously but independently. Coupling the photocatalysts together results in a synergistic enhancement of activity which is likely attributed to factors such as improved electron–hole separation,[61] enhanced light harvesting ability,[62–65] increased surface area,[23] and better CdS film distribution along the inverse opal structure.[66] Additionally, it is interesting to note that although the ternary IO-TiO$_2$–AuNPs–CdS system performed worse than or equal to the binary IO-TiO$_2$–CdS system, it performed the most consistently across both light sources, attaining 67% (Fig. 9A) and 61% (Fig. 9B) degradation in 120 minutes under UV and visible conditions (92% activity retention). By contrast binary IO-TiO$_2$–CdS dropped from 83% (Fig. 9A) to 56% (Fig. 9B) (67% activity retention) and unary CdS from 25% (Fig. 9A) to 12% (Fig. 9B) (48% activity retention). Binary IO-TiO$_2$–AuNPs and unary IO-TiO$_2$ retained 15% (Fig. 9A) and 8% (Fig. 9B) of their UV activity respectively.

3. Experimental

3.1 Materials

Cadmium acetate dihydrate (98%) was purchased from Arcos Organics. Ethylenediaminetetraacetic acid disodium salt dihydrate, (EDTA) (99+%) was purchased from Alfa Aesar. Crystalline ʟ-ascorbic acid (99.6%), Benzoquinone (BQ), and Tertiary-butanol (*t*-BuOH) were purchased from Fischer Scientific. Polyvinylpyrrolidone (PVP) (average MW 40 000 g mol^{-1}), sodium sulfide nonahydrate (98.0%), sodium tetrachloroaurate(III) dehydrate (99%), titanium(IV) bis(ammonium lactate) dihydroxide (50% wt% in H$_2$O) (TiBALDH), styrene monomer, stabilized (99%), 2,2′-azobis(2-methylpropionamidine) dihydrochloride (97%) (AIBA), and trypan blue (TB) were purchased from Sigma-Aldrich. All chemicals and solvents were used as received. Glassware were rinsed with aqua regia (3 : 1 v/v
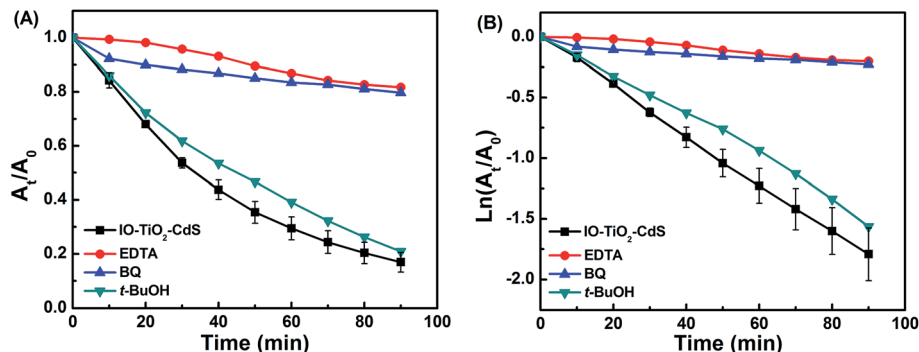
Fig. 8 Photocatalytic activity of the IO-TiO$_2$–CdS for the photocatalytic degradation of TB under UV light in the presence of different scavengers.
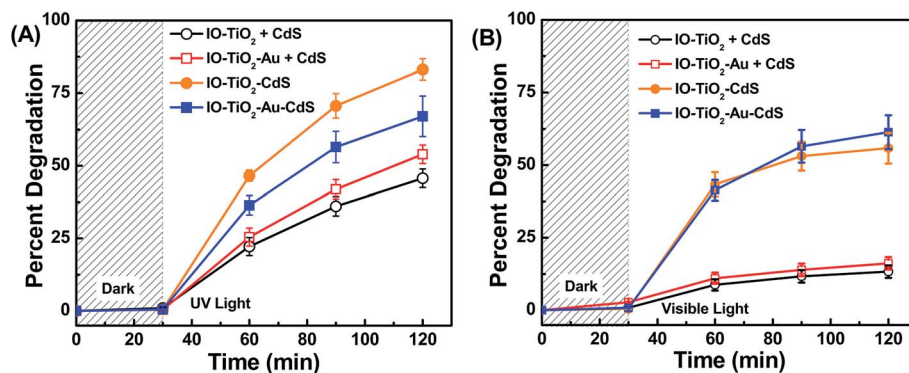

Fig. 9 Synergistic effect for binary and ternary photocatalysts under UV (A) and visible LED (B) irradiation. The binary IO-TiO$_2$–CdS (orange) and ternary IO-TiO$_2$–AuNPs–CdS (green) show higher activity than the sum of their constituent parts IO-TiO$_2$ + CdS (black) and IO-TiO$_2$–AuNPs + CdS (red).

HCl (37%)/HNO$_3$ (65%) solutions) or in base bath (KOH/isopropyl alcohol/H$_2$O) then rinsed thoroughly with DI H$_2$O before use. **Caution:** aqua regia and base bath mixture are dangerous and highly corrosive. Aqua regia and base bath should be used with extreme care. Fresh aqua regia should not be stored in closed containers. The DI water in all experiments was Milli-Q water (18 MΩ cm, Millipore). We have calculated that each of the thin film slides contains 0.2 mg composite materials measured by weighing before and after fabrication.

Our generalized approach is to fabricate the IO-TiO$_2$ composites bottom up by the coassembly of a polystyrene (PS) nanosphere scaffolding with a water soluble titania precursor, TiBALDH followed by calcination of the polymer template and with subsequent deposition of the nanoparticles by *in situ* synthesis and CdS film by SILAR route. A comprehensive procedure is detailed below.

3.2 Synthesis of polystyrene nanospheres

PS nanospheres approximately 270 nm in size were synthesized by surfactant free emulsion polymerization. A 100 mL two necked round bottom flask was placed in a sand bath and fastened with a reflux condenser and a thermometer. The joints were wrapped in Teflon tape to prevent PS from fusing the condenser and the round bottom together during the reaction.

A rubber septum was placed onto the reflux condenser and nitrogen was pumped through a bubbler to create inert atmosphere. Polymerization was carried out by first dissolving 0.0651 g AIBA, 0.6 g PVP, and 5.518 mL styrene in DI water and diluting to 50 mL. The reaction chamber was sealed under nitrogen and slowly heated to 70–80 °C where it was held for 6 hours with stirring. The latex beads were washed by centrifuging at 13 000 rpm for 20 minutes 3–4 times, redispersed in 40 mL DI water, and sonicated for 30 minutes to break up agglomerates.

3.3 Fabrication of inverse opal TiO$_2$

TiO$_2$ inverse opals were made by evaporating a coassembly mixture of polystyrene and TiBALDH in water onto a vertically standing glass substrate.[41,42] Glass microscope slides (0.83 × 1.88 cm) were cut, rinsed with isopropanol and soaked in piranha solution for 30 minutes to make them hydrophilic. The clean slides were stored in DI water and, dried under an N$_2$ stream before use. The coassembly mixture consisted of 1 mL 2.5% wt PS, 160 μL 50% TiBALDH, and was diluted to 4 mL with DI water. One slide was placed in a glass vial (ID ∼ 2 cm) and was submerged in the coassembly mixture. The vials were left in a 45 °C incubator for 1–2 days to evaporate, then were subsequently calcined at 500 °C for 3 hours using a temperature ramp

rate of $2\,°C\;min^{-1}$ in a muffle furnace. After heating, the slides were allowed to cool naturally to room temperature. Films were characterized by SEM, EDX, UV-visible, and Raman spectroscopies.

3.4 *In situ* synthesis of AuNPs

Gold nanoparticles were synthesized *in situ* by the reduction of a gold chloride solution with ascorbic acid. IO-TiO$_2$ slides were taped to the wall of a vial with Kapton tape and immersed in a mixture of 5.940 mL DI water and 60 μL 25 mM NaAuCl$_4$ with stirring. After soaking for 30 minutes, 180 μL of 100 mM L-ascorbic acid was quickly added while stirring was sustained for another 15 minutes, after which the nanoparticle solution was covered and allowed to age overnight.

3.5 CdS deposition by SILAR method

CdS was deposited on plain glass slide or IO-TiO$_2$ or IO-TiO$_2$– AuNPs composites with slight modification of the literature method.[43,44] 50 mM solutions of Cd(CH$_3$COO)$_2 \cdot$2H$_2$O and Na$_2$S$\cdot$9H$_2$O were prepared in ethanol and 25% : 75% water-to-methanol, respectively. The CdS deposition proceeded as followed. First a slide was soaked in the Cd^{2+} solution for 30 seconds before being moved to a beaker containing clean methanol for another 30 seconds. The slide was dried under an N$_2$ stream and then soaked in the S^{2-} solution for 30 seconds. The slide was rinsed again in another beaker of methanol then dried under N$_2$, thereby completing one cycle. SILAR cycles were performed 10 times on clean slides for CdS thin films and on slides containing IO-TiO$_2$ and IO-TiO$_2$– AuNPs.

3.6 Photocatalytic tests

Photocatalytic reactions were performed in an acrylic cuvette. Slides were taped to the side of the cuvette with Kapton tape. 3 mL of 20 μM TB was transferred to the cuvette which was then sealed with parafilm. Cuvettes were left in the dark for 30 minutes to reach adsorption equilibrium before being placed 5 cm away from the visible light source (17 watt white light LED bulb, 1600 lumens, color temperature, 5000 K), in a custom made cushioned sample holder attached to a vortex mixer for solution agitation (Fig. S1†). For UV reactions, a low-pressure mercury UV bench lamp (15 watt, peak wavelength 365 nm) with a 400 nm cutoff filter was used. TB decolorization was monitored by taking a UV-visible spectroscopic measurement every 10 minutes for at least 1.5 hours before stopping the reaction.

3.7 Photocatalytic mechanism studies

Mechanistic studies were carried out for the representative binary IO-TiO$_2$–CdS system in 3 mL 20 μM TB by adding 1 mM EDTA, or BQ, or *t*-BuOH to act as h$^+$, or O$_2^{-\cdot}$, or OH$^\cdot$ scavengers, respectively. Reactions were performed under a UV lamp using a setup identical to the above photocatalytic reaction experiments.

3.8 UV-visible spectroscopic measurements

The absorption spectrum was recorded using a Cary 4000 UV-visible spectrophotometer.

3.9 Raman spectroscopic measurement

Raman spectra were obtained with a portable BWS415-785S i-Raman System produced by BWTEK, equipped with a 785 nm diode laser and BAC-151B video microscope. The software used was BWSpec. The measurements were performed focusing the sample by a 20× objective lens with 8.8 mm working distance (WD). The resolution of Raman shift was <4.5 cm^{-1}. The power of the laser used was 20–60% of the maximum value that was around 320 mW. The integration time of the measurements were 150–5000 ms.

3.10 Electron microscopy and EDX analysis

The material was subsampled and secured to labeled SEM stubs. One piece of 5 mm × 5 mm glass sample was secured to a labeled upper stage. All samples were sputter coated with 15 mm chromium using a Denton DV602 magnetron sputter coater. The samples were imaged using Topcon DS150 Field Emission Scanning Electron Microscope (FE-SEM) at 10 kV in secondary electron mode. EDX data was collected from a JEOL JSM5800LV SEM EDX at an accelerating voltage of 10 keV. Selected area electron diffraction (SAED) pattern was collected using Hitachi H-7600 transmission electron microscope at an accelerating voltage of 120 kV. The sample was prepared by spreading a colloidal solution on an ultra-thin 300 mesh copper grid coated with Formvar/carbon and subsequently dried in the air.

4. Conclusions

In conclusion, we have successfully fabricated binary and ternary 3D macroporous composite thin films namely, IO-TiO$_2$– AuNPs, IO-TiO$_2$–CdS, and IO-TiO$_2$–AuNPs–CdS. The 3D macroporous structure enhanced the dye degradation by augmenting the light-harvesting capabilities. Incorporation of CdS and AuNPs improved the UV light responsive weakness of TiO$_2$ and facilitated the photogenerated electron–hole separation. The introduction of AuNPs between TiO$_2$ and CdS facilitated swift electron transfer between the two and created more active sites in presence of UV light creating a Z-scheme route. Therefore, the ternary composite IO-TiO$_2$–AuNPs–CdS performed better under UV light irradiation than the visible light irradiation. Similarly, the binary IO-TiO$_2$–CdS performed better under UV light than the visible light. In fact, IO-TiO$_2$–CdS under UV light performed best among all the systems and reaction went to completion. Under UV light the composite materials have shown first order kinetics for dye degradation. The photocatalytic degradation of TB under UV light is primarily due to the generation of h$^+$ and the O$_2^{\cdot-}$ radical. Under visible light photogenerated electrons of CdS transferred to the CB of IO-TiO$_2$ with the help of AuNPs. Under UV light the photogenerated electrons of IO-TiO$_2$ are moved to the VB of CdS *via* AuNPs and then recombine with the holes. As we did not observe

significant augmentation of photocatalytic activity due to SPR contribution of AuNPs and observed the photo-corrosion of CdS, further investigation is anticipated with the scope of improved photocatalytic activity.

Conflicts of interest

There are no conflicts to declare.

Acknowledgements

Notes and references

1 L. Sun, R. Zhang, Y. Wang and W. Chen, *ACS Appl. Mater. Interfaces*, 2014, **6**, 14819–14826.

2 P. R. Chowdhury and K. G. Bhattacharyya, *Dalton Trans.*, 2015, **44**, 6809–6824.

3 S. Kuriakose, V. Choudhary, B. Satpati and S. Mohapatra, *Phys. Chem. Chem. Phys.*, 2014, **16**, 17560–17568.

4 J. Liu, L. Zhang, N. Li, Q. Tian, J. Zhou and Y. Sun, *J. Mater. Chem. A*, 2015, **3**, 706–712.

5 S. Rasalingam, C. M. Wu and R. T. Koodali, *ACS Appl. Mater. Interfaces*, 2015, **7**, 4368–4380.

6 V. Vaiano, O. Sacco, D. Sannino and P. Ciambelli, *Appl. Catal., B*, 2015, **170–171**, 153–161.

7 L. Sang, Y. Zhao and C. Burda, *Chem. Rev.*, 2014, **114**, 9283–9318.

8 H. Cai, J. Li, X. Xu, H. Tang, J. Luo, K. Binnemans, J. Fransaer and D. E. De Vos, *J. Alloys Compd.*, 2017, **697**, 132–137.

9 Z. Chamanzadeh, M. Noormohammadi and M. Zahedifar, *Mater. Sci. Semicond. Process.*, 2017, **61**, 107–113.

10 Y. Lai, Y. Tang, J. Gong, D. Gong, L. Chi, C. Lin and Z. Chen, *J. Mater. Chem.*, 2012, **22**, 7420–7426.

11 K. Bhattacharyya, J. Majeed, K. K. Dey, P. Ayyub, A. K. Tyagi and S. R. Bharadwaj, *J. Phys. Chem. C*, 2014, **118**, 15946–15962.

12 E. M. Samsudin, S. B. A. Hamid, J. C. Juan, W. J. Basirun and G. Centi, *Chem. Eng. J.*, 2015, **280**, 330–343.

13 H. Zhao, M. Wu, J. Liu, Z. Deng, Y. Li and B.-L. Su, *Appl. Catal., B*, 2016, **184**, 182–190.

14 Y. Lu, H. Yu, S. Chen, X. Quan and H. Zhao, *Environ. Sci. Technol.*, 2012, **46**, 1724–1730.

15 Y. Zhao, B. Yang, J. Xu, Z. Fu, M. Wu and F. Li, *Thin Solid Films*, 2012, **520**, 3515–3522.

16 T. Butburee, Y. Bai, J. Pan, X. Zong, C. Sun, G. Liu and L. Wang, *J. Mater. Chem. A*, 2014, **2**, 12776–12784.

17 J. Liu, H. Zhao, M. Wu, B. Van der Schueren, Y. Li, O. Deparis, J. Ye, G. A. Ozin, T. Hasan and B.-L. C. Su, *Adv. Mater.*, 2017, **29**, 1605349.

18 X.-Y. Yang, L.-H. Chen, Y. Li, J. C. Rooke, C. Sanchez and B.-L. Su, *Chem. Soc. Rev.*, 2017, **46**, 481–558.

19 M. Zalfani, B. van der Schueren, Z.-Y. Hu, J. C. Rooke, R. Bourguiga, M. Wu, Y. Li, G. Van Tendeloo and B.-L. Su, *J. Mater. Chem. A*, 2015, **3**, 21244–21256.

20 M. Zalfani, B. van der Schueren, M. Mahdouani, R. Bourguiga, W.-B. Yu, M. Wu, O. Deparis, Y. Li and B.-L. Su, *Appl. Catal., B*, 2016, **199**, 187–198.

21 M. Wu, J. Jin, J. Liu, Z. Deng, Y. Li, O. Deparis and B.-L. Su, *J. Mater. Chem. A*, 2013, **1**, 15491–15500.

22 M. Wu, J. Liu, J. Jin, C. Wang, S. Huang, Z. Deng, Y. Li and B.-L. Su, *Appl. Catal., B*, 2014, **150**, 411–420.

23 G. I. N. Waterhouse and M. R. Waterland, *Polyhedron*, 2007, **26**, 356–368.

24 E. S. Kwak, W. Lee, N.-G. Park, J. Kim and H. Lee, *Adv. Funct. Mater.*, 2009, **19**, 1093–1099.

25 D. R. Solli, C. F. McCormick and J. M. Hickmann, *J. Lightwave Technol.*, 2006, **24**, 3864–3867.

26 X. Yang, Z. Peng, H. Zuo, T. Shi and G. Liao, *Sens. Actuators, A*, 2011, **167**, 367–373.

27 M. Wu, Y. Li, Z. Deng and B.-L. Su, *ChemSusChem*, 2014, **4**, 1481–1488.

28 X. Li, X. Chen, H. Niu, X. Han, T. Zhang, J. Liu, H. Lin and F. Qu, *J. Colloid Interface Sci.*, 2015, **452**, 89–97.

29 R. Tong, C. Liu, Z. Xu, Q. Kuang, Z. Xie and L. Zheng, *ACS Appl. Mater. Interfaces*, 2016, **8**, 21326–21333.

30 V. Nguyen, Q. Cai and C. A. Grimes, *J. Colloid Interface Sci.*, 2016, **483**, 287–294.

31 J.-H. Yun, Y. H. Ng, S. Huang, G. Conibeer and R. Amal, *Chem. Commun.*, 2011, **47**, 11288–11290.

32 L. Yang, S. Luo, Y. Li, Y. Xiao, Q. Kang and Q. Cai, *Environ. Sci. Technol.*, 2010, **44**, 7641–7646.

33 Y. Hou, X.-Y. Li, Q.-D. Zhao, X. Quan and G.-H. Chen, *Adv. Funct. Mater.*, 2010, **20**, 2165–2174.

34 B. Pant, N. A. M. Barakat, H. R. Pant, M. Park, P. S. Saud, J.-W. Kim and H.-Y. Kim, *J. Colloid Interface Sci.*, 2014, **434**, 159–166.

35 Y. Xie, G. Ali, S. H. Yoo and S. O. Cho, *ACS Appl. Mater. Interfaces*, 2010, **2**, 2910–2914.

36 P. Zhou, Z. Le, Y. Xie, J. Fang and J. Xu, *J. Alloys Compd.*, 2017, **692**, 170–177.

37 J. Zhang, F.-X. Xiao, G. Xiao and B. Liu, *Appl. Catal., A*, 2016, **521**, 50–56.

38 M. Kim, Y. K. Kim, S. K. Lim, S. Kim and S.-I. In, *Appl. Catal., B*, 2015, **166–167**, 423–431.

39 A. Arabzadeh and A. Salimi, *J. Colloid Interface Sci.*, 2016, **479**, 43–54.

40 G. Song, F. Xin, J. Chen and X. Yin, *Appl. Catal., A*, 2014, **473**, 90–95.

41 B. Hatton, L. Mishchenko, S. Davis, K. H. Sandhage and J. Aizenberg, *Proc. Natl. Acad. Sci. U. S. A.*, 2010, **107**, 10354–10359.

42 Z. Hu, L. Xu, L. Wang, Y. Huang, L. Xu and J. Chen, *Catal. Commun.*, 2013, **40**, 106–110.

43 C. Cheng, H. Wang, J. Li, H. Yang, A. Xie, P. Chen, S. Li, F. Huang and Y. Shen, *Electrochim. Acta*, 2014, **146**, 378–385.

44 L. Xia, L. Xu, J. Song, R. Xu, D. Liu, B. Dong and H. Song, *Sci. Rep.*, 2015, **5**, 10838.

45 J. Oh, Y. W. Chang, H. J. Kim, S. Yoo, D. J. Kim, S. Im, Y. J. Park, D. Kim and K. H. Yoo, *Nano Lett.*, 2010, **10**, 2755–2760.

46 A. L. Schmucker, N. Harris, M. J. Banholzer, M. G. Blaber, K. D. Osberg, G. C. Schatz and C. A. Mirkin, *ACS Nano*, 2010, **4**, 5453–5463.

47 J. S. Jang, S. M. Ji, S. W. Bae, H. C. Son and J. S. Lee, *J. Photochem. Photobiol., A*, 2007, **188**, 112–119.

48 I. Honma, T. Sano and H. Komiyama, *J. Phys. Chem.*, 1993, **97**, 6692–6695.

49 J. Fang, L. Xu, Z. Zhang, Y. Yuan, S. Cao, Z. Wang, L. Yin, Y. Liao and C. Xue, *ACS Appl. Mater. Interfaces*, 2013, **5**, 8088–8092.

50 J. Xian, D. Li, J. Chen, X. Li, M. He, Y. Shao, L. Yu and J. Fang, *ACS Appl. Mater. Interfaces*, 2014, **6**, 13157–13166.

51 G. Liu, H. G. Yang, C. Sun, L. Cheng, L. Wang, G. Q. Lu and H. M. Cheng, *CrystEngComm*, 2009, **11**, 2677–2682.

52 H. Zhu, B. Yang, J. Xu, Z. Fu, M. Wen, T. Guo, S. Fu, J. Zuo and S. Zhang, *Appl. Catal., B*, 2009, **90**, 463–469.

53 I. K. Konstantinou, T. M. Sakellarides, V. A. Sakkas and T. A. Albanis, *Environ. Sci. Technol.*, 2001, **35**, 398–405.

54 C. Guo, M. Ge, L. Liu, G. Gao, Y. Feng and Y. Wang, *Environ. Sci. Technol.*, 2010, **44**, 419–425.

55 Y. Yang, Z. Ma, L. Xu, H. Wang and N. Fu, *Appl. Surf. Sci.*, 2016, **369**, 576–583.

56 H. Tada, T. Mitsui, T. Kiyonaga, T. Akita and K. Tanaka, *Nat. Mater.*, 2006, **5**, 782–786.

57 X. Zhang, Y. Liu, S.-T. Lee, S. Yang and Z. Kang, *Energy Environ. Sci.*, 2014, **7**, 1409–1419.

58 Z. Jiang, D. Jiang, Z. Yan, D. Liu, K. Qian and J. Xie, *Appl. Catal., B*, 2015, **170–171**, 195–205.

59 D. A. Reddy, J. Choi, S. Lee, R. Ma and T. K. Kim, *RSC Adv.*, 2015, **5**, 67394–67404.

60 H. Zhang and Y. Zhu, *J. Phys. Chem. C*, 2010, **114**, 5822–5826.

61 P. Zhou, J. Yu and M. Jaroniec, *Adv. Mater.*, 2014, **26**, 4920–4935.

62 M. Fujishima, Y. Nakabayashi, K. Takayama, H. Kobayashi and H. Tada, *J. Phys. Chem. C*, 2016, **120**, 17365–17371.

63 I. Robel, M. Kuno and P. V. Kamat, *J. Am. Chem. Soc.*, 2007, **129**, 4136–4137.

64 W. A. Tisdale, K. J. Williams, B. A. Timp, D. J. Norris, E. S. Aydil and X. Y. Zhu, *Science*, 2010, **328**, 1543–1547.

65 Y. Wang, D.-B. Xiong, W. Zhang, H. Su, Q. Liu, J. Gu, S. Zhu and D. Zhang, *Catal. Today*, 2016, **274**, 15–21.

66 C. Cheng, S. K. Karuturi, L. Liu, J. Liu, H. Li, L. T. Su, A. I. Y. Tok and H. J. Fan, *Small*, 2012, **8**, 37–42.